

Electromagnetic Catastrophe in Ultrarelativistic Shocks and the Prompt Emission of Gamma-Ray Bursts

Boris E. Stern^{1,2*}

¹*Institute for Nuclear Research, Russian Academy of Sciences, Moscow 117312, Russia*

²*Astro Space Center of Lebedev Physical Institute, Moscow, Profsoyuznaya 84/32, 117997, Russia*

Accepted, Received

ABSTRACT

It is shown that an ultrarelativistic shock with the Lorentz factor of order of tens or higher propagating in a moderately dense interstellar medium (density above $\sim 1000 \text{ cm}^{-3}$) undergoes a fast dramatic transformation into a highly radiative state. The process leading to this phenomenon resembles the first order Fermi acceleration with the difference that the energy is transported across the shock front by photons rather than protons. The reflection of the energy flux crossing the shock front in both directions is due to photon-photon pair production and Compton scattering. Such mechanism initiates a runaway nonlinear pair cascade fed directly by the kinetic energy of the shock. Eventually the cascade feeds back the fluid dynamics, converting the sharp shock front into a smooth velocity gradient and the runaway evolution changes to a quasi-steady state regime. This effect has been studied numerically using the nonlinear Large Particle Monte-Carlo code for the electromagnetic component and a simplified hydrodynamic description of the fluid. The most interesting application of the effect is the phenomenon of gamma-ray bursts where it explains a high radiative efficiency and gives a perspective to explain spectra of GRBs and their time variability. The results predict a phenomenon of “GeV bursts” which arise if the density of the external medium is not sufficiently high to provide a large compactness.

Key words: gamma-rays:bursts – shock waves – methods: numerical

1 INTRODUCTION

Astrophysical objects where we observe (active galactic nuclei) or infer (gamma-ray bursts, soft gamma-repeaters) a relativistic bulk motion demonstrate surprisingly high gamma-ray luminosity. In some cases the energy release in gamma-rays can be comparable to the total kinetic energy of the bulk motion in the source. This implies a very efficient mechanism of the energy conversion of the bulk motion into the hard radiation. It is clear that in the case of explosive phenomena like GRBs the radiation originates from ultrarelativistic shocks (Cavallo & Rees 1978; Rees & Mészáros 1992). This is less certain in the case of AGN jets, however there exist a large number of works considering shocks as the main source of AGN jet radiation (for a review see Kirk, 1997).

One can describe the energy stored in the shock in two ways: as a total kinetic energy of ejecta and shocked matter or as their internal energy. There are known two different ways of shock energy release: the first order Fermi acceleration and different mechanisms of internal energy dissipation. Fermi acceleration does not require the dissipation as it is fed directly by the kinetic energy of

the bulk motion. On the other hand, Fermi acceleration has a number of limiting factors in available power and radiative efficiency (see, e.g., Bednarz & Ostrovsky 1999). With this reason Fermi acceleration is usually considered as a source of high energy cosmic rays while the intensive radiation is traditionally explained in terms of the internal energy dissipation.

This work suggests a highly radiative analog of Fermi acceleration where the main role is played by photons rather than by charged particles. A similar idea about important role of neutral particles in shocks has been suggested independently in a very recent paper by Derishev et al. (2003). For a simple illustration the shock and the external medium can be represented as two mirrors moving with an ultrarelativistic velocity respectively to each other. Let ξ_s and ξ_e be their reflection coefficients (depending on the kind and the energy of a particle) and Γ – the Lorentz factor of the shock. A photon being elastically reflected head-on from a moving mirror gains a factor $\sim \Gamma^2$ in its energy. Thus the total energy of photons participating in back and forth motion between the mirrors can be roughly described by the equation

$$dE/dt = (\xi_s \xi_e \Gamma^2 - S)E/t_c \quad (1)$$

where t_c is a characteristic time of reflection cycle and S is the probability of the particle escape. Actually equation (1) represents

* E-mail: stern@lukash.asc.rssi.ru

not more than an instructive toy model since a real situation is essentially non-local (t_c is uncertain) and require an integration through particle spectra. If $\xi_s \xi_e \Gamma^2 > S$, the total energy of particles will grow exponentially until mirrors decelerate.

In the case of the first order Fermi acceleration the reflection results from the diffusion of supra-thermal charged particles in magnetic field. How this two-mirror approach will look when applied to photons? If a soft photon (e.g. of a synchrotron nature) interacts only with electrons, the reflection coefficients ξ_s and ξ_e are of order of the Thomson optical depth of each medium ($\xi_s \sim \xi_e \sim \tau_T$, see section 2). This case does not differ essentially from the well known thermal Comptonization in relativistic regime at electron temperature $\Gamma - 1$. The photon boosting terminates as soon as the photon gains a sufficient energy to interact in Klein-Nishina regime when reflection coefficients decrease. The Compton boosting is probably not very important by itself, however it could provide photons above pair production cutoff and give rise to a new much more powerful effect.

The importance of pair production in GRB shocks and AGN jets has been emphasized in many works, e.g., by Thompson (1997), Ramires-Ruis et al. (2000) and Mészáros, Ramires-Ruis & Rees (2001). Thompson (1997) and Ramires-Ruis et al. (2000) stated that the pair production can enhance the radiation efficiency of the shock providing new supra-thermal particles as seeds for Fermi acceleration. In this work we show that the pair production plays a crucial role initiating a runaway energy release.

A necessary condition to trigger this process is the existence of a seed radiation field in the vicinity of the shock. This radiation should be dense in terms of the photon number: $n_p R \sigma_T \gg 1$ where R is a characteristic scale, both n_p and R correspond to the comoving frame of the shock where photons are approximately isotropic. Such photons can appear e.g. as the result of an internal energy dissipation and undergo the Compton boosting.

Now let a photon of energy $\varepsilon \gg 1$ (hereafter ε is the photon energy in electron mass units) moves upstream across the shock front. Then, interacting with a soft photon, it produces an e^+e^- pair in unshocked matter ($\xi_e \sim 1$ in this case). The pair is bound to the rest frame of the external matter if the e^+ and e^- Larmor radii do not exceed the scale characterizing the problem. Particles are advected downstream across the shock front, losing a fraction of their energy to Comptonization. Some of downstream Comptonized photons can produce new pairs behind the shock front which in turn upscatter soft photons upstream. So we deal with multiple electromagnetic interactions and the whole process can be characterized as an electromagnetic cascade fed by kinetic energy of two converging media or *cascade boosting*. The energy involved in the cascade can grow exponentially and eventually the process can reach a nonlinear stage when the boosting rate increases.

All above conclusions have been made in assumption that the shock front separating unshocked and shocked media is very sharp and can be characterized as a viscous jump. It is known from studies of nonrelativistic shocks that the viscous jump can disappear transforming into a smoother transition due to radiation pressure ahead the shock. Thompson & Madau (2000) have studied preacceleration of external matter for the case of a GRB external shock and demonstrated that the pair production (pair loading) is extremely important in this respect and feeds back the radiation efficiency. Beloborodov (2002) has considered a more extreme case when the radiation of GRB ejecta sweeps up the external medium far ahead the shock. In that case the energy should be supplied from internal shocks. Our case is closer to that of Thompson & Madau (2000). The preacceleration of external medium transforms the vis-

cous jump into a smoother velocity gradient. This transformation removes the radiative divergence: now an upstream photon most probably interacts in preaccelerated medium and the energy gain in the interaction becomes much less than Γ^2 . We should expect the formation of some steady state regime where the fluid velocity pattern is adjusted in a way to satisfy the energy conservation law. The luminosity at this stage should be close to its ultimate value $L \sim \Gamma^2 dm/dt$ where m is the mass of the external matter swept up by the shock.

Summarizing, we can expect the following evolution: (i) a seed radiation due to dissipation of the internal energy; (ii) Compton boosting and the cascade boosting of the electromagnetic component in linear exponential regime; (iii) a sharper nonlinear evolution when the boosted high energy component contributes to the soft target photon field; (vi) transformation of the shock front and setting up a highly luminous quasi-steady state regime. The entire event is so dramatic that it deserves the name “electromagnetic catastrophe”.

This qualitative illustration is confirmed below at a quantitative level. The main tool in this study is the large particle nonlinear Monte-Carlo (LPMC) code described in Stern et al. (1995).

While the mechanism can work in different astrophysical phenomena this study is focused on its application to GRBs. Correspondingly, the explored region of parameters represents the prevailing view on GRBs (large Lorentz factors, moderate densities).

In Section 2 we describe the general formulation of the problem, the accepted assumptions and the range of parameters. Section 3 briefly describes the approach to the numerical simulations of the effect. Section 4 presents the results of simulation runs demonstrating the evolution of the system from a low luminosity initial state through the catastrophe to a highly radiative post-catastrophe regime. Section 5 extends the range of the phenomenon to lower densities and outlines the threshold where the catastrophe is possible at certain assumptions. Section 6 describes a phenomenon of GeV bursts which should arise when the compactness is insufficient to provide optically thick pair loading. Possible associations with existing data are discussed. In section 7 we discuss various GRB scenario associated with electromagnetic catastrophe and the issue of the GRBs time variability.

2 FORMULATION OF THE PROBLEM

2.1 The simplified description of the shock

For convenience we consider the shock in the comoving system which is preferable for its higher symmetry: the density contrast is moderate (factor 4 in an idealized case), upstream and downstream energy fluxes can be comparable. More explicitly, we bound our reference system to the contact discontinuity, its Lorentz factor hereafter is Γ . The shock front in this frame moves upstream with semirelativistic velocity β_s (hereafter, β is the velocity in units of the velocity of light). We assume that the shocked external matter between the shock front and the contact discontinuity is of a constant density and in rest relatively to the contact discontinuity. Actually this region can be subject to a semirelativistic bulk motion (perhaps with a turbulent component) depending on the distribution of external matter and shock dynamics. Neglecting such motion we remove an additional source of the free energy and since we are interested in an explosive energy release this is a conservative assumption.

We do not know and do not consider the state of ejecta behind

the contact discontinuity, prescribing to it a role of a heavy piston, carrying the main fraction of the kinetic energy. It is assumed that ejecta does not emit or reflect radiation. Actually ejecta can contribute the seed radiation and the downstream-upstream reflectivity.

We assume a spherical symmetry at least within a cone of opening angle $1/\Gamma$ respectively to the line of sight. Due to relativistic effects we almost do not observe the emission of the shock beyond this cone. Events in the shock separated by angle more than $1/\Gamma$ are not causally connected since the acceleration stage. Most probably the ejecta is strongly beamed within a solid angle $\Omega \ll 1$, we exclude Ω from the consideration using the isotropic equivalents for global energy parameters: the kinetic energy of ejecta, E , and the luminosity, L . The actual energetics is then described by ΩE and ΩL .

The spherical shock viewed from the comoving system is parabolically curved and the matter moves outward from the line of sight, relativistically at the angular displacement $\sim 1/\Gamma$ from the line of sight. For simplicity we adopt one-dimensional slab geometry with no bulk motion in the axial direction. This is not a conservative simplification because in this way we violate kinematic and causality constraints on interactions of photons emitted from distant regions of the shock. In order to avoid this problem, the consideration was restricted to a comparatively small time (less than a half deceleration time) when the above constraints are still not important.

The unshocked interstellar matter (ISM) in the comoving system is a cold fluid with bulk Lorentz factor Γ . The ordered particle motion dissipates into chaotic motion with the same average thermal Lorentz factor Γ when the fluid crosses the shock front. The energy density contrast across the front and the front velocity in the comoving system, β_s , result from the energy conservation:

$$U_s \beta_s = U_o (\beta + \beta_s), \quad (2)$$

where U_s is the energy density of the shocked matter, β is the external fluid velocity, $U_o = \Gamma^2 \rho m_p c^2$, ρ is the rest frame ISM number density, and from the pressure – momentum balance:

$$P_s = \frac{1}{3} U_s = U_o \beta (\beta + \beta_s). \quad (3)$$

In the ultrarelativistic limit ($\beta = 1$) equations yield $\beta_s = 1/3$ $U_s = 4U_o$. For a more detailed description of a relativistic shock see Blandford & McKee (1976).

The thickness of the shock (between the shock front and the contact discontinuity) at the constant external density and spherical geometry is $\Delta X = \frac{1}{12} R/\Gamma$ in the comoving system.

2.2 Main parameters and dimensionless units

External magnetic field H_e is different for cases of the stellar wind dominated and the ISM dominated environments. In the first case, the field is predominantly radial and processes leading to the catastrophe are inhibited (ξ_e is very low) unless the field is affected by radiation front ahead the shock. Most probably it must be affected by the two stream instability generating a chaotic component. Moreover, a spherical asymmetry of the environment and ejecta together with the charge asymmetry (Compton scattering on electrons) can induce a large scale transversal field similar to that induced in an atmospheric nuclear explosion.

In the ISM dominated case, the field originally should have a large scale geometry and a substantial transversal component. In this work only the ISM case is studied quantitatively, note that the

interaction of the shock with a slow shell of matter ejected by a GRB progenitor essentially does not differs from the ISM case. ISM magnetic field depends on the external density ρ and the reasonable assumption is this case is $H_e \sim 10^{-5} \sqrt{\rho} \text{ G}$, where ρ is in cm^{-3} units. Hereafter we treat H_e as the transversal component.

The lower limit for the magnetic field in the shock H follows from Lorentz transformation and the compression by factor 4: $H > H_g = 4H_e \Gamma$. However, this field can be much stronger being generated at the shock. At this step we can rely on numerical study of the two stream instability by Medvedev & Loeb (1999). According to their simulations the ensured value of energy density of generated field, U_B , is $\sim 0.01 - 0.1$ of electron energy density in the shock, U_e , and, tentatively, the field can be amplified up to $U_B \sim 0.01 - 0.1$ of proton energy density.

The parameters of the problem are: initial Lorentz factor Γ , total kinetic energy E , external number density ρ , characteristic rest frame size R , seed luminosity of soft photons L_s , their spectrum, values of magnetic field in both regions, H (shock) and H_e . As a reasonable hypothesis for the seed spectrum we accept a power law $dN/d\varepsilon \propto \varepsilon^\alpha$, in the range $\varepsilon_1 < \varepsilon < \varepsilon_2$ (see §2.3).

In the case of GRBs the isotropic kinetic energy of ejecta can vary within two orders of magnitude or more. Maximal observed hard X-ray – gamma-ray GRB energy release is $\sim 5 \cdot 10^{54}$ erg. We accept $E = 10^{54}$ erg as a baseline. In this work we study the case of a constant external density which is a reasonable starting point. The scale of the problem can be characterized by the deceleration radius (Rees & Mészáros 1992):

$$R_d = \left[E / (m_p c^2 \frac{4}{3} \pi \rho \Gamma^2) \right]^{1/3} = 0.24 \cdot 10^{16} E_{54}^{1/3} \rho_6^{-1/3} \Gamma_2^{-2/3} \text{ cm} \quad (4)$$

In the spherical geometry, the scale changes as the shock propagates, therefore we adopt $R = 0.5R_d$ which approximately describes the shock propagation between $0.5R_d$ and R_d . Using the rest frame scale R we can define dimensionless distance, x , and time, t , to work within the comoving system: $x = X/(R/\Gamma)$, $t = T/(R/\Gamma c)$, where X and T are comoving distance and time. Note that the allowed working range is $x < 1$ and $t < 1$. The time in observer frame is $T_{\text{obs}} = tR/(2\Gamma^2 c)$.

It is convenient to describe the energy budget in terms of dimensionless compactness. The latter defines the importance of pair production and, more generally, the level of nonlinearity of the system. The simplest way to introduce this parameter is via the energy column density through the system normalized to the electron mass and multiplied by Thomson cross section:

$$\omega = \frac{U}{m_e c^2} \sigma_T \frac{R}{\Gamma}, \quad (5)$$

where U is an energy density in the comoving system. Particularly, the magnetic compactness is:

$$\omega_B = \frac{H^2}{8\pi m_e c^2} \sigma_T \frac{R}{\Gamma}. \quad (6)$$

This is the compactness describing the energy content of the system. Traditionally the compactness is expressed through the luminosity of the system L :

$$\ell = \frac{L \sigma_T}{R m_e c^3}. \quad (7)$$

The rest (observer) frame compactness for the ultrarelativistic shock is meaningless since the radiation is strongly collimated. The parameter has the stated above physical meaning only in the shock comoving system where particles have a wide angular distribution. Assuming the comoving size of the system R/Γ (with the

transversal size of the same order, see §2.1) and substituting L by the luminosity flux: $L \sim F(R/\Gamma)^2$, with the accuracy of the order of π one gets:

$$\ell = \frac{F}{m_e c^3} \sigma_T \frac{R}{\Gamma}. \quad (8)$$

The total energy budget in the comoving frame constitutes the kinetic energy flux of the fluid crossing the shock front. The corresponding dimensionless expression, kinetic compactness, is:

$$\ell_o = \rho \Gamma^2 m_p c^3 \frac{\sigma_T}{m_e c^3} \frac{R}{\Gamma} = \tau_T \frac{m_p}{m_e} \Gamma. \quad (9)$$

Hereafter we denote energy compactness as ω and the luminosity (power) compactness as ℓ , and $\ell = d\omega/dt$.

2.3 Seed radiation

The seed radiation in the shock can be contributed by (i) the synchrotron – self-Compton radiation of shocked electrons which have the thermal Lorentz factor Γ ; (ii) other channels of internal energy dissipation (e.g. dissipation of magnetic field, plasma waves, turbulence); (iii) external (partially side-scattered) photons from the fireball and a progenitor star; (iv) high energy seed photons associated, e.g. with Fermi acceleration and photo-meson production.

The most confident source is (i) unless synchrotron radiation of shocked electrons is strongly self-absorbed. Its fraction in the total energy budget is limited by the factor m_e/m_p . At some parameters, this seed radiation is sufficient to start the evolution leading to the catastrophe (see Section 3). In such case we deal with the most conservative “minimal hypothesis”. At other parameters the minimal hypothesis is insufficient for the catastrophic evolution. Then we have to consider additional channels of internal energy dissipation (ii) or external photons (iii) and (iv). We would like to avoid a serious consideration of corresponding mechanisms in this work and use a very moderate *ad hoc* hypothesis of the seed soft photon field.

As a baseline, we accept the compactness of such emission $\ell_s \sim \tau_T \Gamma$ which is only m_e/m_p fraction of the total energy budget. The model spectrum of this seed radiation has been taken as a power law fragment with $-2.5 < \alpha < -1.5$ (a free parameter) in the range between ε_1 (typically $\varepsilon_1 \sim 10^{-8}$ which is close to the self-absorption cutoff at $H \sim 100$ G) and ε_2 (a free parameter). Such weak seed radiation is sufficient to give rise to the catastrophe in the most of trials described in this work. The situations when the effect implies a stronger seed radiation are discussed in section 7.

2.4 Reflection of the energy flux

Reflection of a particle flux from the external environment and from the shock is of a primary importance for the cascade boosting (see Eq. 1). Here we consider the reflection of a high energy component of the electromagnetic cascade where the direct Compton reflection of photons is inefficient. In this case the reflectivity of the medium is due to photon-photon generated pairs gyrating in the magnetic field. The requirement that an electron can change its direction to the opposite without a substantial energy loss is a serious limiting factor for the boosting rate.

In the case of the first order Fermi acceleration the main process responsible for the particle scattering upstream across the shock is the diffusion in a chaotic magnetic field (for a recent review see Gollant 2002). In our case the charged particle does not

need to cross the shock, it is sufficient if it just changes its direction upstream. Then photons Comptonized by the particle moving upstream can cross the shock. The deflection of a particle from downstream to upstream hemispheres is a much more probable event than its diffusion upstream the shock, required for Fermi acceleration. Indeed, in the comoving frame of the shocked matter the shock front moves ahead semirelativistically, with $\beta_s = 1/3$, and a charge particle has to diffuse upstream faster.

The downstream – upstream reflection of a particle can proceed in the following ways:

(i). If the Larmor radius is less than the correlation length of the magnetic field, the particle turns at a half Larmor orbit. This can be the case for particles of a moderate energy.

(ii). If the Larmor radius exceeds the correlation length, the particle diffuses in the chaotic field.

(iii). Except the chaotic field H there could exist a large scale component, resulting from a large scale external magnetic field due to the flux conservation: $H_g \sim 4H_e \Gamma$. Then a high energy particle can turn around at a half Larmor orbit in the field H_g . Processes (ii) and (iii) are competing and the leading one depends on concrete parameters. In this work only the effect of the global component has been taken into account since the latter should exist in the adopted model of the external environment. The effect of the diffusion is the matter for future studies.

The reflection efficiency depends on the fraction of energy which the particle loses before it turns around upstream. The energy loss rate is described by

$$-d\gamma/dX = \left(\frac{H}{8\pi} + U_{\text{ph}} \right) \frac{\sigma_T}{m_e c^2} \gamma^2 = C \gamma^2, \quad (10)$$

where X is the comoving distance. The equation yields

$$\gamma(X) = \gamma_o / (1 + \gamma_o X C), \quad (11)$$

where

$$C = H^2 (1 + U_{\text{ph}}/U_B) 3.3 \cdot 10^{-20} \text{ cm}^{-1}. \quad (12)$$

where U_B and U_{ph} are energy densities of magnetic field and soft radiation field respectively. The term U_{ph}/U_B describes the relative contribution of Compton losses. From equation (11) one estimates the maximum energy of downstream – upstream reflected particle $\gamma_{\text{max}} \sim 1/XC$. Substituting X by the half Larmor orbit

$$\pi R_L = 5.3 \cdot 10^3 \frac{\gamma_{\text{max}}}{H_g} \text{ cm}, \quad (13)$$

one obtains the final expression for the maximal energy of a reflected particle:

$$\gamma_{\text{max}} = 0.75 \cdot 10^8 \frac{H_g^{1/2}}{H} (1 + U_{\text{ph}}/U_B)^{-1/2}. \quad (14)$$

The downstream – upstream reflection is inefficient if $U_{\text{ph}}/U_B \ll 1$. Then the main energy of an electron is emitted as a relatively soft synchrotron radiation rather than a hard Comptonized photons. The limiting energy of synchrotron photons emitted by an electron after half Larmor orbit is $\varepsilon \sim 200$ at $H_g \sim H$. This energy is still sufficient for pair production, however the cascade boosting in this case will be substantially slower and the compactness threshold for the electromagnetic catastrophe will be higher. In this work we study the case of low H and weak dissipation. If the generated field is much stronger but its dissipation into electromagnetic component is fast, then we have $U_{\text{ph}}/U_B \sim 1$ again. The boosting is inhibited if the field is strong and its dissipation is slow ($U_{\text{ph}} \ll U_B$).

In the case of the external environment (upstream-downstream reflection) the electron synchrotron losses are small. Indeed, in the rest frame equation (14) with $H_g = H = 10^{-5} \sqrt{\rho}$ yields

$$\gamma_{r,\max} = 1.3 \cdot 10^{10} \rho_6^{-1/2} (1 + U_{\text{ph}}/U_B)^{-1/2} \quad (15)$$

where the subscript r refers to the rest frame and $\gamma_{\max} \sim \Gamma \gamma_{r,\max}$. The term U_{ph}/U_B is large in the external environment, (i.e. Compton losses are much larger). However, Comptonized photons have predominantly downstream direction and contribute to the cascade boosting.

The main limiting factor in upstream – downstream reflection is the requirement that the Larmor radius should be smaller than the characteristic size of the problem. Actually, the upstream particle can be advected back across the shock front when it deflects by just the angle $1/\Gamma$. In this case it has a much less energy gain than Γ^2 . Both effects were accounted for in the numerical simulation. From the limit on the gyroradius $R_L < R$ equations (4) and (13) yield:

$$\gamma_{r,\max} < 1.4 \cdot 10^{12} H_e E_{54}^{1/3} \rho_6^{-1/3} \Gamma_2^{-2/3}. \quad (16)$$

Using the hypothesis $H_e = 10^{-5} \sqrt{\rho}$ and transforming to the comoving frame one gets:

$$\gamma_{\max} < 1.4 \cdot 10^{11} E_{54}^{1/3} \rho_6^{1/6} \Gamma_2^{1/3}. \quad (17)$$

Note that the limits (14) and (16) have an opposite dependence on the magnetic field. A faster boosting takes place in the case of a stronger external field and a weaker field in the shock. The above estimates are given for the orientation while the numerical simulation reproduces directly the particle trajectory and the energy loss along it. The quantitative effect of these parameters on the boosting rate and examples of upstream and downstream particle spectra are demonstrated in Section 5.

3 MONTE-CARLO SIMULATIONS

The entire problem outlined above is too difficult for an analytic treatment. In this work it is studied numerically using a Large Particle Monte-Carlo code (LPMC) developed by Stern (1985) and Stern et al. (1995). The code is essentially nonlinear: the simulated particles constitute at the same time a target medium for other particles. Large particle (LP) method in this application means that each simulated particle represents w real particles (for GRBs $w > 10^{50}$). The most reasonable weighting scheme except some special cases is to set $w\varepsilon = \text{const}$, where ε is the energy of the particle and the constant can vary since the total energy involved in the simulation can change. The number of LPs was $2^{17} = 131072$.

The version of LPMC used here treats Compton scattering, synchrotron radiation, photon-photon pair production, and pair annihilation. Synchrotron self-absorption was neglected as it consumes too much computing power and is not very important in this application. All these processes are reproduced without any simplifications at the microphysics level. On the other hand, a number of serious macroscopic simplifications has been done.

Since the number of large particles which is limited by the computing power available at the moment did not allow full three-dimensional simulation, the problem was reduced to one dimension, x , along the shock propagation. While locations and momenta of LPs were three dimensional, the target density was averaged over slab layers and the fluid representation was one-dimensional.

The trajectories of electron and positrons in the magnetic field were simulated directly assuming transversal geometry of the field

H_g in the shock and H_e in the external matter. Thus the problem of the reflection qualitatively discussed in §2.4 was implemented in the numerical simulation. Protons were assumed to be cold in the fluid frame unless they have crossed the dissipative shock front.

Hydrodynamic part of the problem becomes very difficult since the energy and momentum transferred by LPs to the fluid fluctuate. Attempts to simulate the fluid with internal pressure have led to rising instabilities at semirelativistic velocities. Therefore a dust approximation (where the internal fluid pressure is neglected) has been adopted and the fluid velocity behind the shock front was artificially fixed to zero.

The dust approximation works satisfactory until the fluid has a moderate temperature and energy density in its comoving frame (i.e. when it is ultrarelativistic in the shock comoving frame). This circumstance was used by Beloborodov (2002) and Thompson & Madau (2000) who also described the preacceleration of the external medium by the radiation front in terms of dust approximation. The approximation does not work at all in the shock where the pressure at a relativistic temperature is comparable to the radiation pressure. The adopted hydrodynamic ansatz allows to describe the effect in general and fails to account for possible interesting effects associated with semirelativistic motion behind the radiation front. The approach can be considered as a “zero approximation”.

4 EVOLUTION OF THE SYSTEM THROUGH THE CATASTROPHE

To illustrate qualitative arguments discussed in Introduction with numerical simulations, we present results of two runs with different parameters. First, for Lorentz factor $\Gamma = 100$ and the density of external environment $\rho = 3 \cdot 10^5 \text{ cm}^{-3}$. Second, for $\Gamma = 30$, $\rho = 10^6 \text{ cm}^{-3}$. Other parameters for these cases are $R = 1.9 \cdot 10^{15} \text{ cm}$, $\ell_o = 63$, $T_o = 3.1 \text{ s}$ and $R = 2.8 \cdot 10^{15} \text{ cm}$, $\ell_o = 94$, $T_o = 52 \text{ s}$. The first case is closer to the traditionally assumed value of Γ for GRBs, however it is more difficult for numerical treatment since statistical fluctuations associated with finite number of large particles being amplified by factor Γ^2 . With this reason the first run tracks the evolution of the system only till the beginning of the post-catastrophe stage.

Initial state is empty of photons and consists only of fluid of cold protons and electrons with bulk Lorentz factor Γ , representing external medium viewed from the comoving system. Seed photons appear as the (partially self-absorbed) synchrotron radiation of shocked electrons. In this case, the self-absorption is not very strong and can be ignored. The Comptonization of the synchrotron peak gives second and third peaks at higher energies (further Comptonization is inefficient because it proceeds in Klein-Nishina regime). These peaks are visible in Figure 1 at $t = 0.3$. The Comptonized photons are produced both by shocked and external electrons. The latter cause an anisotropy: the second peak is stronger in downstream photons (Figure 1, lower panel), while the third peak is slightly more intensive upstream (Figure 1, upper panel).

At $t = 0.4$ a high energy tail appears due to pair production by photons of the third peak in the external medium (which provides comoving energy gain by factor Γ^2). Then, around $t = 0.5$, the evolution accelerates dramatically, the total energy of photons rises by more than 3 orders of magnitude (the power supplied to photons jumps by factor $\sim m_p/m_e$), and the spectrum transforms from harder to softer one. The evolution from $t = 0.49$ to $t = 0.52$ will take about 0.1 second from the point of view of an external ob-

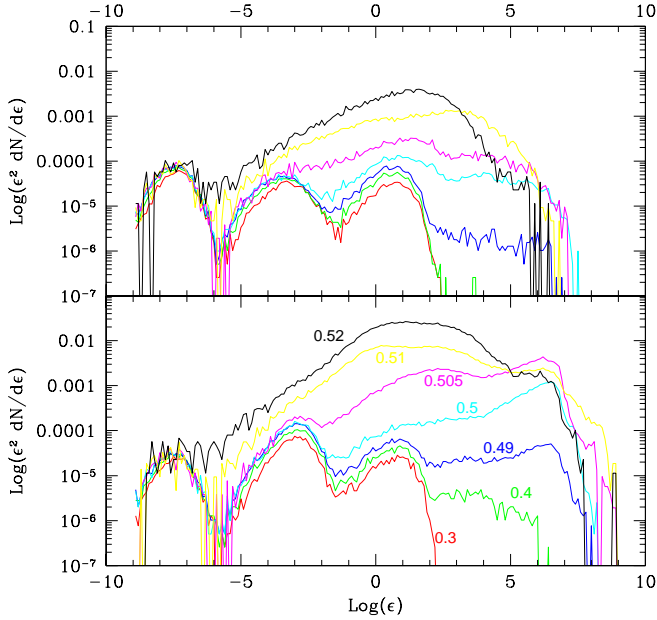


Figure 1. Instantaneous spectra of photons for $\Gamma = 100$, $\rho = 3 \cdot 10^5 \text{cm}^{-3}$ during pre-catastrophe and catastrophe stages. Upper panel shows the upstream and lower – the downstream photon spectra. Labels in the lower panel indicate the dimensionless time from the start of the simulation. Curves in the upper panel correspond to the same time sequence. Time unit corresponds to 3.1 s in the observer frame.

server. The simulation has been terminated at $t = 0.56$ because numerical problems associated with the high Lorentz factor become further serious. These problems are not principal and can be overcome just with the increase in the computing power. The evolution of the system with time is shown in Figure 3.

This example does not require any additional source of energy except the bulk kinetic energy of the fluid and any external photons. In this sense the case can be interpreted as a “minimal model”, however one still has to assume a non-radial external magnetic field.

The case of $\Gamma = 30$, $\rho = 10^6 \text{cm}^{-3}$ does require additional assumptions. First of all, the synchrotron radiation of electrons with $\varepsilon = 30$ is deeply self-absorbed. Therefore an internal energy source accelerating a fraction of shocked electrons up to $\varepsilon \sim 200 - 300$ is required. The required power is, nevertheless, much less than the total energy budget: $\ell_s \sim m_e/m_p \cdot \ell_o$. To avoid extra details we just ignored the self-absorption since the nature and energy of seed photons is not very important. Another problem is that the energy of the second Comptonization peak is smaller than in the previous example and the catastrophe develops too slowly. In section 5 it is shown that a much faster evolution can be induced by seed high energy photons which population undergoes an exponential breeding. In this run a portion of upstream high energy photons with total energy compactness $\omega_s \sim 10^{-5}$ (which is $\sim 10^{-7}$ of the total energy budget) has been injected at $t = 0.25$. Then the catastrophe has followed at $t \sim 0.3$.

Figure 2 shows post-catastrophe photon spectra which can be treated as a continuation of the spectra set presented in Figure 1 to later ages. Figure 4 shows the spatial distribution of main quantities: the energy density of upstream photons, the pair number distribution and the bulk Lorentz factor. At the moment of the catastrophe

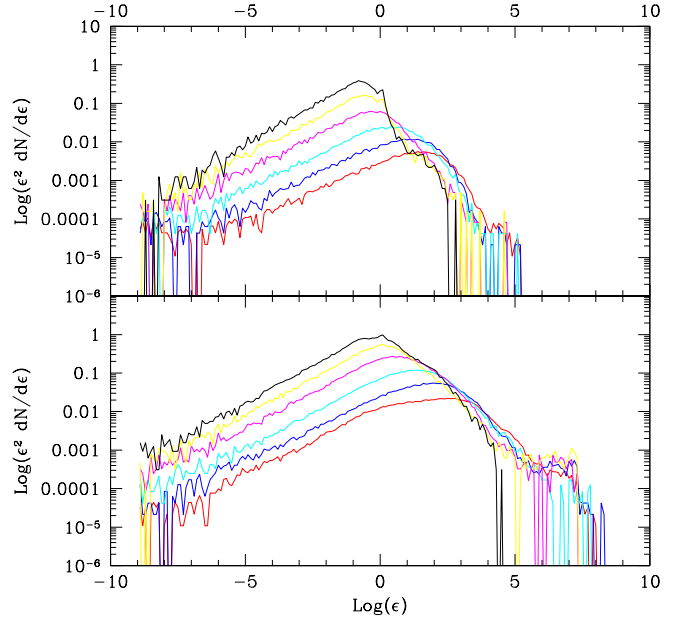


Figure 2. Instantaneous spectra of photons for $\Gamma = 30$, $\rho = 10^6 \text{cm}^{-3}$ during catastrophe and post-catastrophe stages. Upper panel shows the upstream and lower shows the downstream photon spectra. The dimensionless time, from lower to upper curves, is: 0.285, 0.29, 0.31, 0.34, 0.4, 0.5, 0.67. Time unit corresponds to 52 s in observer frame.

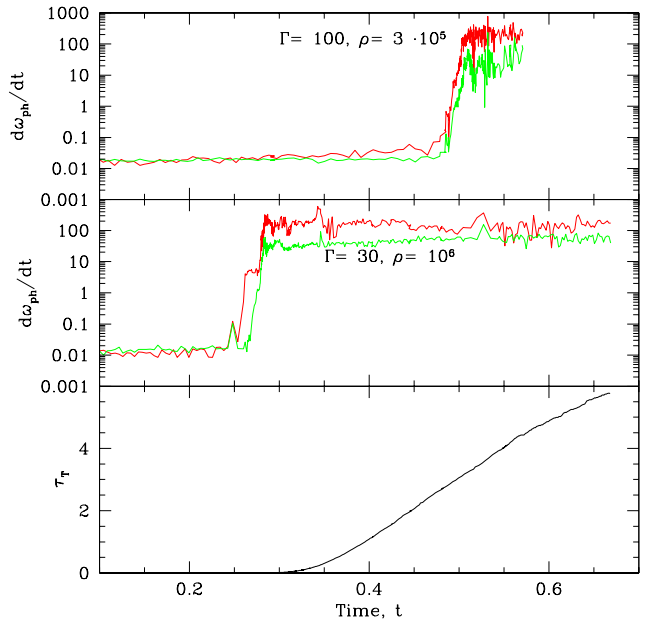


Figure 3. The evolution of the electromagnetic component with time. Upper panel shows the time derivative of the total dimensionless energy $d\omega_{ph}/dt$ of upstream (lower curve) and downstream $d\omega_d/dt$ (upper curve) photons for $\Gamma = 100$, $\rho = 3 \cdot 10^5 \text{cm}^{-3}$. Middle panel: the same for $\Gamma = 30$, $\rho = 10^6 \text{cm}^{-3}$. Lower Panel shows the evolution of pair Thomson optical depth for $\Gamma = 30$, $\rho = 10^6 \text{cm}^{-3}$.

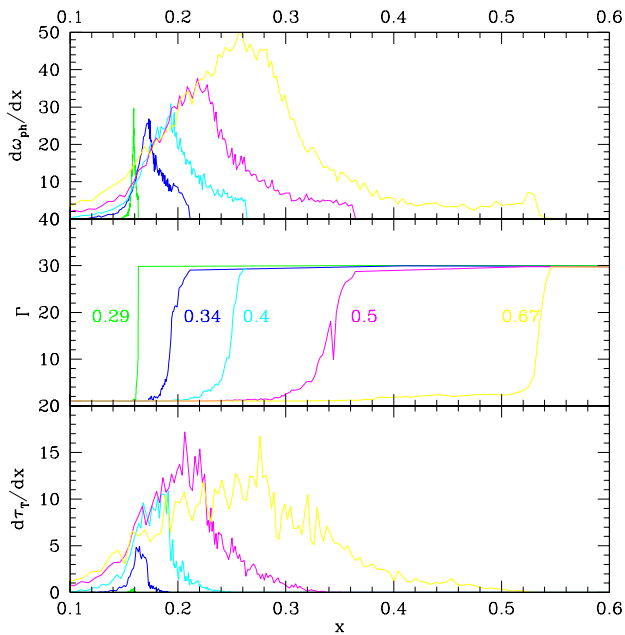


Figure 4. The distributions of the upstream photon energy density, the bulk Lorentz factor and the pair number density across the shock (upper, middle and lower panels respectively). $x = 0$ corresponds to contact discontinuity. Labels indicate the dimensionless time since the start of the simulation.

trophe the main fraction of photon energy is tightly concentrated to the fluid velocity jump which has a step-like character (see Figure 4, upper and middle panels, curve at $t = 0.29$). The reason is that the evolution at that moment is so fast, that abruptly released photons have no time to disperse wider. Then photons disperse and a leading fraction of them form a radiation front moving with the speed of light. The distribution of the bulk Lorentz factor smooths and adjusts to the radiation front (Fig. 4, middle panel) moving ahead with a near-luminal velocity. The absence of a viscous jump at the post-catastrophe stage means that new protons join the shock being cold: they are smoothly decelerated (or accelerated in the rest frame) by radiative reaction via pairs and magnetic field.

The fluid behind the main radiation front (where it has a semirelativistic velocity) is not pressure balanced in this approximation. The thermal pressure of protons at $x < 0.15$ swept up before the catastrophe exceeds the radiation pressure of downstream photons. This disbalance should affect the velocity distribution and a real pattern can be more complicated. One can expect a semirelativistic forward bulk motion at the left from the broad peak of the photon distribution, which will compress and push pair-photon gas ahead.

As far as the model is very simplified and works progressively worse in attempts to trace the evolution further, we terminate the simulation at $t = 0.67$. At the present level without a careful hydrodynamic treatment we are not able to study shock deceleration stage and cannot reproduce the final time profile of the radiation. We also cannot say when and how the highly radiative post-catastrophe state terminates.

In order to represent results in terms of observed gamma-ray emission we have to consider different photon components in the comoving system:

(a). The downstream component which takes the main frac-

tion of the momentum and the energy of the decelerating external medium, after the viscous shock front disappears. Its energy is related to the mass of the external medium m swept up after the catastrophe as $E_d \sim mc^2\Gamma$.

(b). The upstream component (which is actually isotropic in the comoving frame) results from the absorption and quasi-isotropic reemission of the downstream flux: $E_u \sim \eta E_d$ where η is the average opacity of the system for the downstream photon flux. After the transformation of the upstream component to the rest (observer) frame we have:

$$E_{u,o} \sim \eta mc^2 \Gamma^2 \quad (18)$$

The opacity rises during the evolution and approaches unity in the case of the high compactness. Indeed, all soft photons scatter in optically thick layer of pairs, while hard photons are absorbed due to pair production. The deceleration of the shock can be roughly described as

$$\frac{d\Gamma}{dm} = -\eta \frac{\Gamma^2}{M} \quad (19)$$

Where M is the invariant mass (comoving energy) of the shock. Note that at $\eta < 1$ the deceleration is slower than in adiabatic case which is described in the same way as (19) at $\eta = 1$.

It is remarkable that the upstream spectrum evolves towards a GRB-like spectral shape, however still does not reach it. The peak energy of the latest spectrum in Fig. 2 is around 70 keV. When blueshifting the spectrum to the observer frame and assuming a cosmological redshift $z = 1$ the peak energy comes out around 1 MeV. There exist GRBs with such peak energy, however the typical peak energy is less - between 200 and 300 keV. The low energy slope in this example is $\alpha \sim -1.5$ while for a typical GRB $\alpha \sim -1$. The values of the peak energy and α resulting from this run are quite robust: the peak energy comes out from transition from Thomson to Klein-Nishina regime in Compton scattering on nonrelativistic or semirelativistic electrons, $\alpha = -1.5$ corresponds to cooling spectrum of relativistic electrons (see e.g. Ghisellini, Celotti, & Lazatti 2000).

Summarizing, one should conclude that at the present level the model does not reproduce GRB spectra. Nevertheless, the phenomenon provides a perspective to address the problem due to efficient pair production and generation of optically thick layer of pairs behind the radiation front (see Fig. 3 and Fig. 4, lower panels). Once we have an optically thick pair plasma, we can expect that it will produce a thermal Comptonization peak which may describe GRB spectra (Thompson 1997, Ghisellini & Celotti 1999, Liang 1999). In this simulation such peak cannot be reproduced since cooled pairs are not Maxwellized: their energy distribution is in Compton equilibrium with the photon spectrum. This is a consequence of the simplified approach omitting various processes of potential importance. Particularly, the spectra could be modified in a proper direction by thermal bremsstrahlung and double Compton scattering (for a review see Thompson 1997).

Actually, cool pairs should be subject to a variety of collective phenomena, i.e. dissipation of plasma waves or turbulence. As the result a prominent Comptonization peak can appear. Note, that the asymptotic case of the Comptonization peak is Wien distribution which is much harder in low energy part ($\alpha = +2$) than GRB spectra. A partially developed Wien peak could be a promising solution of the problem.

The contradiction in the location of the spectral break ϵ_p can be relaxed if the initial Lorentz factor of the shock is 20 - 40 rather

than 100 – 300 and the peak luminosity being emitted by a partially decelerated shock.

5 EXPONENTIAL BOOSTING OF A SEED HIGH ENERGY COMPONENT

The first example in Section 4 presents a full nonlinear simulation of the system without any initial seed photons. Here we show that the existence of a very small amount of high energy photons at the start extends the possible range of the catastrophic evolution down to a much lower external density than it was probed in Section 4. The most suitable source of such photons is Fermi acceleration of protons with photo-meson production and possible $p-n$ conversion suggested by Derishev et al. (2003).

Because of a high computing cost of the full nonlinear simulation in this section we explore the parameter space simulating the cascade boosting in a linear regime using linearized version of LPMC code. This means that the target LP field is not affected by the simulated high energy component. A high boosting rate ensures that the system evolution eventually reaches the catastrophe stage even at a small seed amount of high energy photons.

During the boosting, the spectrum of the high energy component evolves until it reaches some steady state shape that we do not know *a priori*. Therefore we have to perform a full simulation of the high energy component tracking its growth to a sufficiently long time. Then, in order to handle an exponential branching of the cascade tree we have to use statistical weights: to cut some branches compensating this by an increase of the statistical weight of remaining branches. The main technical problem in this simulation is large fluctuations in cascade histories which have a very slow convergence when we accumulate the average history. Since the seed target photon field has an upper cutoff at ε_2 the high energy component was simulated down to the lower cutoff $1/\varepsilon_2$: photons below this cutoff do not produce pairs.

Magnetic field and the seed (target) radiation field were taken according to §§2.2 and 2.3. The parameters of the seed spectrum were frozen at $\alpha = -2$ and $\varepsilon_2 = 10^{-4}$. With this assumptions we reduce the parameter space to two dimensions: Γ and ρ . Because the assumptions are not obvious, it would be reasonable to accept the following strategy: to explore Γ, ρ space with the standard set of assumptions and, at one point, to defreeze other parameters and to estimate the effect of their variation.

The average breeding time profiles for $\Gamma = 50, \rho = 10^4 \text{ cm}^{-3}$ corresponding to the first three lines in Table 1 are shown in Fig. 5. One can see a confident exponential rise in the number of hard photons crossing the shock upstream. The results on the breeding rate for $\Gamma = 50, \rho = 10^4$ with different sets of other parameters are summarized in Table 1.

	“Nonstandard” parameters	S_{14}	R/S
1	Standard set	5.5	21.0
2	$H_e = 0.2H_e^o$	31.	4.8
3	$H_e = 5H_e^o$	2.4	48.2
4	$\omega_B = 10\omega_B^o$	37.	3.1
5	$\omega_B = 0.1\omega_B^o$	2.0	58.8
6	$\alpha = -1.75$	2.9	40.3
7	$\alpha = -1.5$	5.1	23.0
8	$\alpha = -2.25$	21.0	2.5
9	$10^{-8} < \varepsilon < 10^{-3}$	4.7	25.0
10	$10^{-8} < \varepsilon < 10^{-5}$	15.3	7.6

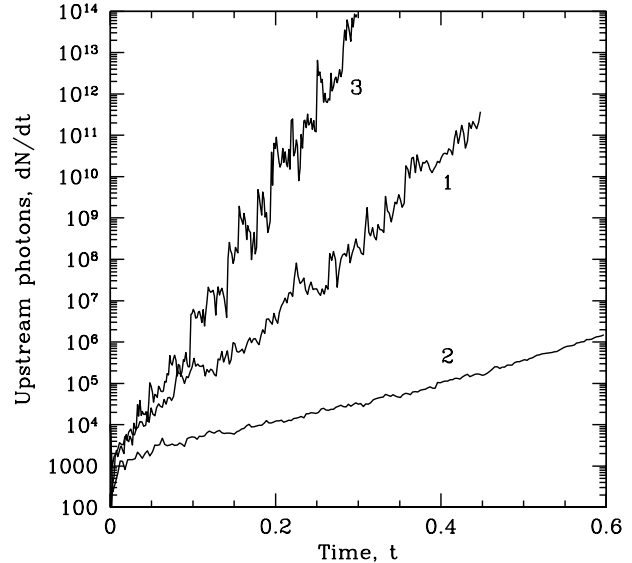


Figure 5. Average breeding time histories for $\Gamma = 50, \rho = 10^4 \text{ cm}^{-3}$ and different external magnetic field. Labels indicate corresponding line numbers in Table 1.

Table 1 The boosting rate of the high energy component for $\Gamma = 50, \rho = 10^4$ ($\ell_o = 7.3$) depending on other parameters. Second column gives those parameters which differ from the standard set (see text). Third column shows the boosting rate in terms of the distance of the shock propagation S where the high energy component grows by an order of magnitude. Fourth column gives the total growth of the high energy component (orders of magnitude) when the shock propagates the distance $R = 0.5R_d = 1.17 \cdot 10^{16} \text{ cm}$, where the deceleration distance R_d implies the initial isotropic kinetic energy 10^{54} erg . The standard parameters are: $\ell_e = 3.5 \cdot 10^{-3}$, $H^o = 14.7 \text{ G}$, $\omega_B^o = 1.4 \cdot 10^{-3}$, $H_e^o = 10^{-3} \text{ G}$, $\varepsilon_2 = 10^{04}$, $\alpha = -2$

First of all it should be noticed that the breeding rate at moderate parameters $\Gamma = 50, \rho = 10^4 \text{ cm}^{-3}$ is in a large excess over required to trigger the catastrophe in the most of trials. One can see a strong dependence on magnetic field. The effects of H and H_e variation are of opposite signs as it was qualitatively shown in §2.4.

Figure 6 demonstrates spectra of particles crossing the shock (energy of all particles is in the comoving system). One can see that the main fraction of energy is transferred downstream across the shock by high energy Comptonized photons rather than by advected pairs. The turnover in spectra of upstream photons qualitatively agrees with equation (14) yielding $\gamma_{\text{max}} \sim 3 \cdot 10^6$ for $\rho = 10^4$ and $\gamma_{\text{max}} \sim 0.7 \cdot 10^7$ for $\rho = 10^3$. A larger difference in these two cases visible in Fig. 6 appears due to a higher pair production opacity for high energy photons in the first case.

Fig. 7 demonstrates the map of $\Gamma - \rho$ space when other parameters are frozen as described above. Levels of the constant compactness and the constant time scale are given for total isotropic kinetic energy $E = 10^{54} \text{ erg}$. Both compactness and the time scale vary as $E^{1/3}$ in the spherical geometry and at the constant density. The broken solid line shows the catastrophe threshold which is conventionally defined as the condition that the cascade is boosted at least by 10 orders of magnitude when the shock propagates the distance $R = 0.5R_d$. Perhaps one could use a weaker requirement: we prefer to use this conservative criterion since the real intensity of the seed high energy radiation is unknown.

The threshold line in Fig. 7 depends on the frozen parameters,

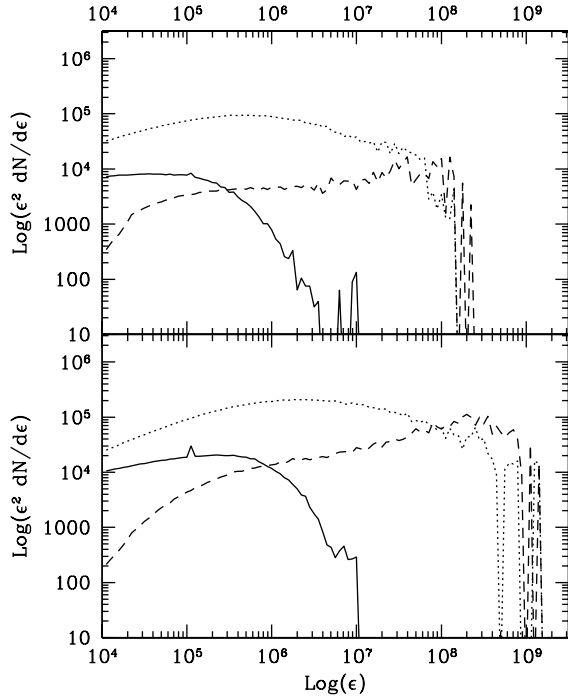


Figure 6. Spectra of particles crossing the shock for $\Gamma = 50$, $\rho = 10^4 \text{cm}^{-3}$ (upper panel) and $\Gamma = 50$, $\rho = 10^3 \text{cm}^{-3}$ (lower panel) and standard set of other parameters. Solid lines: upstream photons; dotted lines: downstream photons; dashed lines: downstream pairs. Spikes at $\epsilon = 10^5$ represents monochromatic photons injected at $t = 0$.

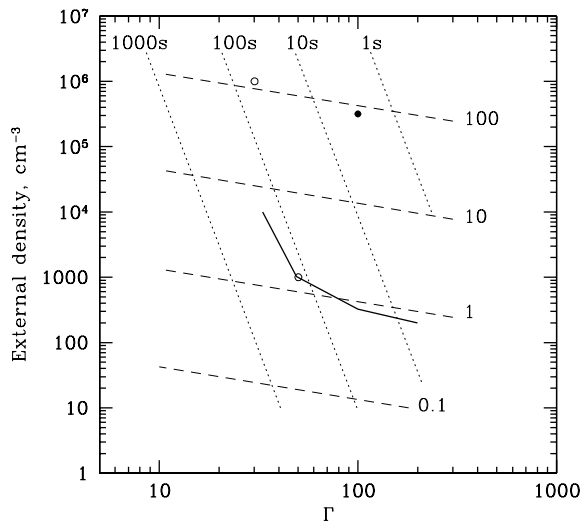


Figure 7. The explored area in $\Gamma - \rho$ coordinates (other parameters are frozen as described in the text). The solid line shows the threshold for the catastrophe estimated with the conventional condition that the seed high energy component grows at least by 10 orders of magnitude as the shock propagates the distance $R = 0.5R_d$. Dashed lines represent the levels of the constant observer time scale $R/(\Gamma^2 c)$ and dotted lines correspond to the constant comoving compactness ℓ_o assuming $E = 10^{54}$ erg. Circles represent parameters for full nonlinear simulation runs described in Sections 4 and 6.

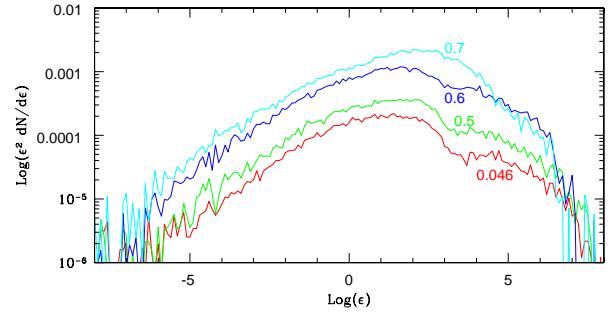


Figure 8. Instantaneous spectra of photons for $\Gamma = 50$, $\rho = 10^3 \text{cm}^{-3}$. Labels indicate the dimensionless time t from the start of the simulation. Time unit corresponds to 133 s in the observer frame.

i.e. it is model dependent. As it was mentioned in §2.4 the strong slowly dissipating magnetic field in the shock would substantially rise the threshold. On the other hand if the field dissipates very fast leaving a dominating large scale component, the threshold would be lower. The range of the catastrophe would be extended if an external field stronger than assumed is induced due to spherically asymmetric Compton drag as discussed in §2.2.

6 GEV BURSTS

Two runs described in Section 4 correspond to a comparatively high compactness parameter when the main energy release occurs in the soft gamma range. In Section 5 it is shown that the catastrophe is possible at a much less compactness (see Fig. 7). In such case we can expect to observe a much harder radiation which would approximately correspond to early spectra in Fig.1. In order to demonstrate this directly we performed a run for $\Gamma = 50$, $\rho = 10^3 \text{cm}^{-3}$. The compactness is $\ell_o = 1.1$, “standard” magnetic field in the shock $H = 4.4$ G, characteristic radius $R = 2.0 \cdot 10^{16} \text{cm}$, observer time scale $T_o = 133$ s. The “minimal model” does not work at such parameters as the primary synchrotron radiation is strongly self-absorbed, therefore the same standard ad hoc hypothesis of the seed radiation as in Section 5 has been used: $l_s = \ell_o m_e/m_p$, $10^{-8} < \epsilon < 10^{-4}$, $\alpha = -2$. The catastrophe at such parameters develops due to the breeding of external high energy photons. It was assumed that the high energy component due to preceding breeding has gained the luminosity $\omega_h = 0.005\omega_s \sim 2.5 \cdot 10^{-6} \ell_o$. The corresponding amount of upstream high energy photons with $\epsilon = 10^5$, has been injected at the start of the simulation.

The resulting sequence of instantaneous upstream photon spectra is shown in Fig. 8. Generally, at a low compactness we can expect a maximum of $\epsilon^2 dN/d\epsilon$ distribution in high energies and an approximate power law spectrum in a wide range with the index between $\alpha = -1.5$ (fast cooling spectrum) and $\alpha = -2$ (saturated pair cascade, Svensson, 1987). In this case the maximum energy release is at the rest frame energy ~ 5 GeV (the spectrum in Fig 8 is not final, however, since some hardest photons will be absorbed on the way to the observer).

According to Fig. 7, the catastrophe threshold at $\Gamma \sim 50$ is $\ell_o \sim 1$ when the main energy is still released in hard gamma-rays. This value is model dependent, the threshold can be higher for less favorable combination of parameters, e.g. for higher ω_B/ω_s ratio. Nevertheless, if the environment of GRB progenitors is diverse, we can expect that GeV bursts should be as usual phenomenon as clas-

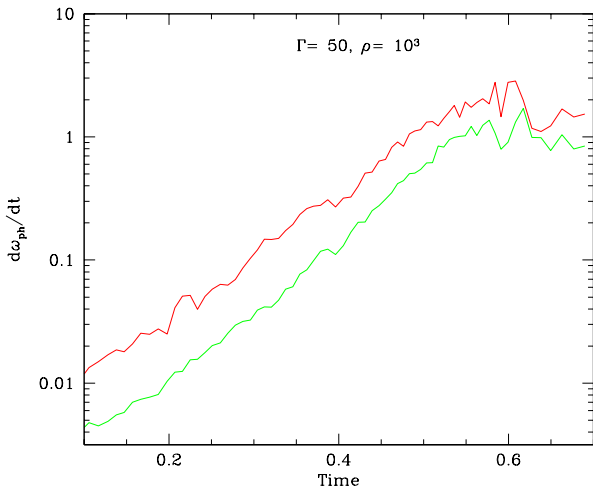


Figure 9. The evolution of the electromagnetic component with time for $\Gamma = 50$, $\rho = 10^3 \text{ cm}^{-3}$. The time derivative of the total energy of upstream (lower curve) and downstream (upper curve) photons is shown.

sic GRBs. On the other hand, they are more difficult for observations. Such events should be weaker in soft gamma range (soft gamma fluence is one – two orders of magnitude less than the high energy fluence). And, more importantly, they should be longer and smoother (see Figs. 7 and 9). The example of this section corresponds to characteristic time scale 133 s (the total duration can be longer). Such events are more difficult for a triggering and an off-line search than classic GRBs, unless an event is strong enough. The long duration also makes difficult a time-location cluster analysis for high energy photons in existing data.

Has something like this been observed? A candidate for such a GeV burst is GRB 970417a detected simultaneously by BATSE and Milagro (Atkins et al. 2000) in the range above 50 GeV. The inferred fluence above 50 GeV is at least an order of magnitude greater than the fluence in the BATSE range which corresponds to the type of the spectrum shown in Fig. 8 if the maximum is at an order of magnitude higher energy. However, it was a comparatively short burst with $T_{90} = 7.9$ s. Then following Fig. 7 one has to assume a high Lorentz factor ($\Gamma \sim 200$), or a less kinetic energy at a lower Γ . Note that there should be a strong selection effect in favor of short GeV bursts.

Another hint at GeV bursts provide EGRET data. The famous GRB 940217 (Hurley et al. 1994) where EGRET has detected a delayed GeV emission during an hour after BATSE trigger hardly can match the concept of a GeV burst. It rather looks like a superposition of a classic GRB and a GeV burst. In principle this is possible when the shock meets localized dense clouds while propagating in a less dense environment. Better candidates for GeV bursts can be several EGRET detected GRBs reported by Catelly, Dingus & Schneid (1997) and Dingus, Catelly & Schneid (1997). Some of them have high energy spectral indices $\alpha \sim -2$ up to GeV range. Eventually the issue of GeV bursts will be clarified by GLAST mission.

7 DISCUSSION

While the effect of the electromagnetic catastrophe can, in principle, be applied to different astrophysical phenomena, its application

to GRBs is of the highest interest. Below we discuss the main issues where the effect can be relevant.

7.1 The radiative efficiency and the GRB scenario

The considered effect straightforwardly provides the ultimate ($\sim 100\%$ radiation efficiency and, in this respect, it probably has no competing mechanisms. The phenomenon of GRBs does require a high radiation efficiency. The total isotropic soft gamma ray energetics of GRBs with measured redshift varies between 10^{52} and $5 \cdot 10^{54}$ erg. A low efficiency would imply much higher values for the isotropic kinetic energy of the ejecta which probably contradicts the afterglow data.

The catastrophe is a model independent effect which, however, has a set of threshold conditions. If GRBs were associated with coalescence of neutron star binaries, the effect would never work since the expected density of the environment is too low: $0.1 - 1 \text{ cm}^{-3}$. However a wealth of recent data support the collapsar scenario where we can expect a much higher density and the phenomenon may occur (see Mészáros 2002 for a review). Is it possible that the threshold conditions are still never satisfied despite a sufficient density of the environment? Formally, it could be if the external magnetic field is always purely radial. But as it was discussed in §2.2 the radial field structure can hardly survive the early stage of a GRB in any scenario. Other inhibiting factor could be a strong domination of magnetic energy density over radiation energy density. However, we do observe GRBs implying a high radiation density in the source. Whatever produces this radiation at the start should end up with the electromagnetic catastrophe.

The effect is associated mainly with external shock scenario as internal shocks have too low relative Lorentz factor. On the other hand, internal shocks can radiate only a relatively small fraction of the total kinetic energy because of kinematic constraints. A competition with a much more efficient mechanism presents a new difficulty for the internal shock scenario. For example, let us consider the typical internal shock scenario: prompt GRB emission from $R \sim 10^{13} - 10^{14}$ cm due to collisions of multiple shocks and the following afterglow due to an external shock at larger radii. An important modification to this scenario introduces the effect discovered by Beloborodov (2002): the radiation emitted by internal shocks sweeps out the external matter up to radius $R \sim 10^{15} - 10^{16}$ cm leaving an empty cavity. Now let us consider the situation when the shock reaches the edge of the cavity. It meets the environment with enhanced density and optical depth (since the swept out matter is compressed and loaded by a large amount of pairs), with a non-radial magnetic field (the radial field structure can hardly survive such event), with intense seed radiation (side scattered photons). These are perfect conditions to give rise to the electromagnetic catastrophe with a proper GRB time scale. If so, the radiative energy release in such collision would outshine a burst from internal shocks by 1.5 – 2 orders of magnitude (the main fraction of total kinetic energy of the ejecta at the full radiative efficiency versus a few per cent of the kinetic energy at unknown radiative efficiency). This would look as the main event, rather than the afterglow. Even if the main energy release is in the GeV range (low compactness, see Section 6), such events can hardly escape systematic observations.

7.2 Issue of the time variability

The internal shock model is motivated mainly by difficulties with description of the GRB time variability arising in the external shock scenario (Fenimore 1996). Dermer (2000), on the other hand, suggests a number of possible solutions for external shocks. The effect of the electromagnetic catastrophe may extend the list of possible solutions.

1. The catastrophe is a nonlinear effect which can amplify any fluctuations in external density and seed radiation. In addition it is sensitive to the geometry of magnetic field. One dimensional treatment performed in this work loses many important features which could appear in a 3D simulation with realistic hydrodynamic treatment. The catastrophe most probably will develop locally in many spots within $1/\Gamma$ cone at different time. The spherical symmetry of the shock should be distorted due to a strong feedback between the radiation and the fluid pattern. As a result one can observe a complex time structure even at an approximate symmetry in the initial state.

2. The post-catastrophe evolution was interpreted here as a quasi-steady state. Actually, especially in the case of decreasing density, it could be unstable and recurrent. This could be, e.g., due to a version of the Beloborodov effect: the radiation of external shock passing through the dense matter sweeps out a less dense matter ahead, radiation decays until the shock catches up the swept matter. Then the shock regenerates producing a new emission episode. In this way one can explain episodes separated by long quiescent intervals.

3. The spherical symmetry of ejecta can be completely broken prior the emission stage up to fragmentation into a bunch of separate droplets of different transversal size $X_T < R/\Gamma$ (this implies a hydrodynamic transversal confinement of droplets which needs a separate study). This requires a strong instability (most probably of Rayleigh-Taylor type) at some stage. A model representing a GRB ejecta as a shower of blobs was proposed by Heinz & Begelman (1999). This is the most attractive possibility because in addition to the complex time structure it can produce a chain reaction: the catastrophe in one droplet supply seed photons to a neighboring droplet and induce the next catastrophe. It was shown by Stern & Svensson (1996) that the chain reaction gives a statistical and qualitative description of GRBs temporal diversity.

All these suggestions require 3D numerical studies.

7.3 Problem of the spectral break

The observed spectral break in the sub-MeV range with a very hard low energy slope is still a serious problem. It seems that this problem is common for all GRB models assuming a high Lorentz factor and a small optical depth. Two alternative explanations of the spectral break for optically thin emitting medium were suggested: optically thin synchrotron emission in slow cooling regime and synchrotron self-absorption break. For the criticism of the former see Ghisellini, Celotti & Lazatti (2000). The latter implies too high magnetic field (in our case the self-absorption break should appear at $\varepsilon \sim 10^{-6} - 10^{-5}$ in observer frame).

As it was discussed in Section 4 the electromagnetic catastrophe at a high compactness provides an optically thick pair loading and thus gives a perspective to explain the break with thermal Comptonization peak. However there remains the issue whether the thermal Comptonization is sufficiently fast and efficient. If it works, then we should find an anticorrelation between the sharpness of the break (implies high compactness) and the high energy emission

(implies low compactness). If the break is still too persistent then we have to conclude that our consideration misses some important detail. For example, a possible role of ejecta behind the contact discontinuity was ignored while actually it could be an efficient photon reflector.

The location of the break hints at a comparatively low Lorentz factor and therefore a high density and small deceleration radius. It could be that the range of parameters studied in this work is actually far from the typical GRB “working regime”.

7.4 Summary

The effect of the electromagnetic catastrophe outlined here in the “zero approximation” can explain the high radiative efficiency of ultrarelativistic shocks while the explanation of the GRB time variability and spectra still require a lot of work. The study of the time variability should certainly rely on a detailed three dimensional hydrodynamics. The understanding of the spectra requires a more complete description of the shock structure and physics of particle interactions for nonrelativistic and semirelativistic pairs.

ACKNOWLEDGMENTS

The author thanks K. Hurley, A. Illarionov, P. Ivanov, J. Poutanen for useful discussions and Y. Tikhomirova for assistance. This work was supported by the Russian Foundation for Basic Research (grant 00-02-16135). A part of this work was done during a visit to the University of Oulu with the support of the grant from the Jenny and Antti Wihuri foundation.

REFERENCES

- Atkins R., et al. 2000, *ApJ*, 533, L119
 Bednarz J., Ostrowski M., 1999, *MNRAS*, 310, L11
 Beloborodov A.F., 2002, *ApJ* 565, 808.
 Blandford R.D., McKee C.F., 1976 *Phys Fluids* 19, 1130
 Catelli J. R., Dingus B. L., Schneid, E. J., 1998, in Meegan C.A., Preece R.D., Koshut T.M., eds, AIP conference proceedings, 428.,
 Gamma-Ray Bursts : 4th Huntsville Symposium, Huntsville, p 309
 Cavallo G, Rees M.J., 1978, *MNRAS*, 183, 359
 Derishev E.V., Aharonian F.A., Kocharovsky V.V., Kocharovsky V.I., 2003, *astro-ph/0301263*
 Dermer C.D., 2000, *astro-ph/0001389*
 Dingus B. L., Catelli J. R., Schneid, E. J., 1998, in Meegan C.A., Preece R.D., Koshut T.M., eds, AIP conference proceedings, 428.,
 Gamma-Ray Bursts : 4th Huntsville Symposium, Huntsville, p 349
 Fenimore E., Madras C.D., Nayakshin S., 1996, *ApJ*, 473, 998
 Ghisellini G., Celotti A., Lazatti D., 2000, *MNRAS*, 313, L1
 Ghisellini G., Celotti A. 1999, *A&AS* 138, 527
 Heinz S., Begelman M.C., 2000, *ApJ*, 535, 104
 Hurley K., et al. 1994, *Nature*, 372, 652
 Kirk J.G., 1997, in Ostrowski M., Sikora M., Madejski G., Begelman M., eds, *Relativistic Jets in AGNs, Proceedings of the International Conference, Krakow* p. 145
 Liang E., 1999, *A&AS*, 138, 529
 Medvedev M.V., Loeb A., 1999, *ApJ*, 526, 697
 Mészáros P., 2002, *ARA&A*, 40, 137
 Mészáros P., Ramirez-Ruiz E., Rees M.J., 2001, *ApJ* 554, 660
 Ramirez-Ruis E., Madau P., Rees M.J., Thompson C., 2001, in Costa E., Frontera E., Hjorth J., eds, *Gamma-Ray Bursts in the Afterglow Era, Proceedings of the International workshop, Rome, Berlin Heidelberg: Springer*, p. 278. .
 Rees M.J., Mészáros P., 1992, *MNRAS*, 258:L41

12 *Boris E. Stern*

Stern B.E., 1985 *Astron Zh*, 62, 529

Stern B.E., Begelman M.C., Sikora M., Svensson R., 1995, *MNRAS*, 272, 291

Stern B.E., Svensson R., 1996, *ApJ*, 469, L109

Svensson R., 1987, *MNRAS*, 227, 403

Thompson C., Madau P. 2000, *ApJ* 538, 105

Thompson C., 1997, in Ostrovski M., Sikora M., Madejski G., Begelman M., eds, *Relativistic Jets in AGNs*, Proceedings of the International Conference, Krakow, p. 63